

QCD Aspects of Hadron Physics*

W. Weise^a

^aPhysik-Department
Technische Universität München
D-85747 Garching, Germany

Several topics in hadron physics at different scales of resolution are discussed. First, deep-inelastic scattering from nucleons and nuclei is viewed in a light-cone coordinate space picture. Then the smooth transition from parton to hadron degrees of freedom is demonstrated by analysing generalized Q^2 -dependent polarizabilities of the nucleon. Turning to low energy QCD we summarize recent developments related to the role of strange quarks in Chiral $SU(3)$ Dynamics, a non-perturbative coupled channel approach to hadronic processes. Finally we elaborate on a unification of QCD Sum Rules with aspects of spontaneous chiral symmetry breaking in the analysis of quark-antiquark excitations of the condensed QCD vacuum and in nuclear matter.

1. Introduction

QCD has a comparatively "simple" basic Lagrangian but offers an enormous variety of physics phenomena. They extend from asymptotically free quarks and gluons at short space-time distances to complex hadronic excitations at larger scales, built on a highly non-trivial vacuum which hosts strong quark and gluon condensates. Given the genuine non-perturbative features of QCD, namely confinement and spontaneous chiral symmetry breaking, the persistent challenge is to identify and explore the active (effective) degrees of freedom at each different scale. The present talk summarizes several topics and recent results related to these issues. We start with an instructive little exercise, elaborating quark and gluon distributions of nucleons and nuclei in coordinate rather than momentum space. Such a description gives a simple geometrical interpretation of the mechanisms at work in deep-inelastic lepton scattering. Turning to lower Q^2 we outline the smooth transition from partonic to hadronic degrees of freedom by the example of generalized (Q^2 -dependent) electromagnetic polarizabilities of the nucleon. Next we move to low-energy QCD with strange quarks. We discuss recent developments and results of Chiral $SU(3)$ Dynamics, our non-perturbative coupled channel approach based on the chiral low-energy effective Lagrangian. In the final part of this survey, the QCD Sum Rule method is unified with aspects of spontaneous chiral symmetry breaking in an attempt to establish

*Dedicated to Koichi Yazaki on the occasion of his 60th birthday; invited talk presented at the KEK-Tanashi Symposium on Physics of Hadrons and Nuclei, Tokyo, December 14–17, 1998. Work supported in part by DFG and BMBF

model-independent constraints for vector meson spectra, both in vacuum and in nuclear matter.

2. Deep-inelastic lepton scattering in coordinate space

Nucleon structure functions are commonly analyzed in momentum space. In coordinate space, quark and gluon distributions are defined as correlation functions involving two field operators separated by a light-cone distance $y^+ = t+z = 2l$. In deep-inelastic scattering as viewed in the laboratory frame with the target nucleon or nucleus at rest, the longitudinal distance $y^+/2$ entering in the parton correlation function can be compared with length scales characteristic of nucleons and nuclei and offers new insights into the nature of parton distributions and their interpretation.

The quark and gluon distributions are expressed in terms of the squared four-momentum transfer Q^2 and the Bjorken variable $x = Q^2/2M\nu$, where M is the nucleon mass and ν is the energy transfer in the lab frame. In the Bjorken limit the dominant contributions to the structure functions at small Bjorken- x come from the light-like separations of order $y^+ \sim 1/Mx$. Consequently, large longitudinal distances $l = y^+/2 = (2Mx)^{-1}$ are important in the scattering process at small x .

The space-time pattern of deep-inelastic scattering is then as follows: the virtual photon interacts with partons which propagate a distance y^+ along the light cone. The characteristic lab frame correlation length l is half of that distance. These features are naturally implemented in coordinate space (so-called Ioffe time) distribution functions [1]. In accordance with their properties under charge conjugation one introduces these coordinate space distributions as one-dimensional Fourier sine and cosine transforms of the momentum space quark and gluon distributions:

$$\mathcal{Q}(y^+, Q^2) = \int_0^1 dx \sin\left(\frac{My^+}{2}x\right) [q(x, Q^2) + \bar{q}(x, Q^2)], \quad (1)$$

$$\mathcal{Q}_{valence}(y^+, Q^2) = \int_0^1 dx \cos\left(\frac{My^+}{2}x\right) [q(x, Q^2) - \bar{q}(x, Q^2)], \quad (2)$$

$$\mathcal{G}(y^+, Q^2) = \int_0^1 dx \cos\left(\frac{My^+}{2}x\right) x g(x, Q^2). \quad (3)$$

Consider first the coordinate space parton distributions of a free nucleon. We start from realistic input distributions using the CTEQ4L parametrization [2] at $Q_0^2 = 1.4 \text{ GeV}^2$, perform the QCD (DGLAP) evolution to $Q^2 = 4 \text{ GeV}^2$ and then take the Fourier transforms (1–3) to translate the distributions into coordinate space. The result [3] is shown in Fig. 1. Note that $\mathcal{Q}(y^+, Q^2)$ and $\mathcal{G}(y^+, Q^2)$ extend to distances far beyond the diameter of the nucleon. In fact they grow continuously, reflecting the strong rise of the structure function $F_2(x, Q^2)$ observed at $x < 10^{-3}$. Even the valence quark distribution has a pronounced tail extending beyond the nucleon size. The interpretation in the lab frame is simple: at very small Bjorken- x corresponding to large longitudinal distances the virtual photon converts into a beam of partons which propagate along the light cone and interact with partons of the target nucleon, probing its sea quark and gluon content. This "beam" stretches over length scales much larger than the size of the nucleon itself. The partonic

composition of that beam is dominated by a steadily growing number of gluons at larger distances.

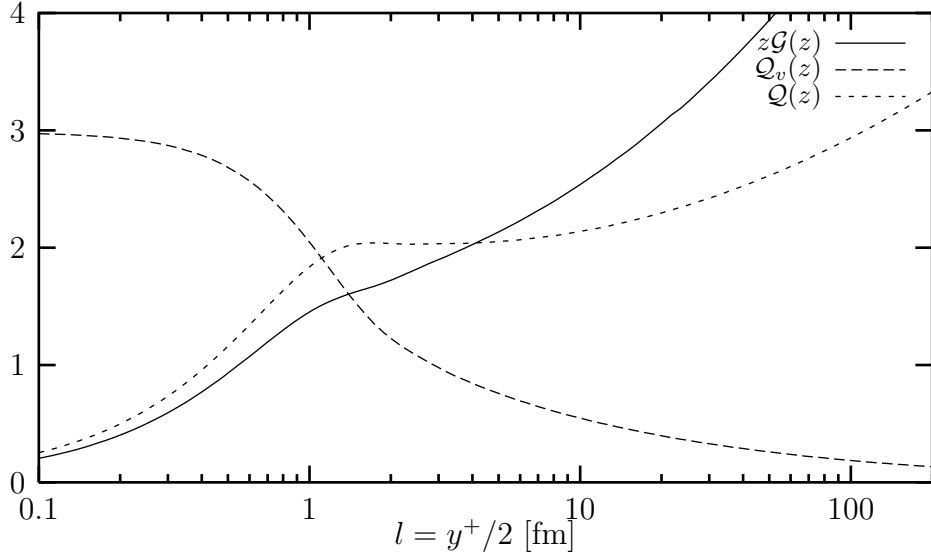


Figure 1. Coordinate space quark and gluon distributions at $Q^2 = 4 \text{ GeV}^2$. Dashed curve: Valence quarks; dotted curve: total quark and antiquark distribution; solid curve: gluons. For details see ref. [3].

It is instructive to examine parton distributions of nuclei using the same picture. A detailed momentum space analysis of these distributions has been performed in refs. [4], combining data from deep-inelastic lepton-nucleus scattering and Drell-Yan lepton pair production in proton-nucleus collisions. Based on these data the quark and gluon content of the nuclear distributions was extracted using a DGLAP evolution analysis. One can then take the ratio of Fourier transforms of the nuclear and free nucleon distributions:

$$\mathcal{R}(y^+, Q^2) = \frac{\mathcal{Q}^A(y^+, Q^2)}{\mathcal{Q}^N(y^+, Q^2)} \quad (4)$$

for quark distributions, and analogous ratios for gluon distributions. Nuclear effects can now be analysed in coordinate space. The result [3] shown in Fig. 2 for ^{40}Ca clearly demonstrates the most prominent features. Effects of binding and Fermi motion which modify the structure functions at longitudinal distances $l = y^+/2$ smaller than the nucleon diameter ($l < 2 \text{ fm}$) are evidently marginal. The leading effect is shadowing, the reduction of the ratios \mathcal{R} substantially below one, due to coherent multiple scattering of the parton "beam" from at least two nucleons in the target nucleus. This effect starts as soon as the propagation length of quark and gluon fluctuations of the virtual photon exceeds the average distance between nucleons in the nucleus ($l > d \simeq 2 \text{ fm}$). The interesting feature is again the prominent role of gluons in this process. The measured shadowing effect is

represented by the ratio \mathcal{R}_{F_2} of the corresponding F_2 structure functions for nuclei and free nucleons. This ratio reflects the shadowing effect on the sum of quark and antiquark distributions seen directly by the virtual photon. The indirect effect of gluon shadowing, expressed in terms of the ratio $\mathcal{R}_g = \mathcal{G}^A(y^+, Q^2)/\mathcal{G}^N(y^+, Q^2)$, is obviously very strong. While this ratio is not directly observable, it certainly indicates a large effective cross section for gluons interacting with nucleons.

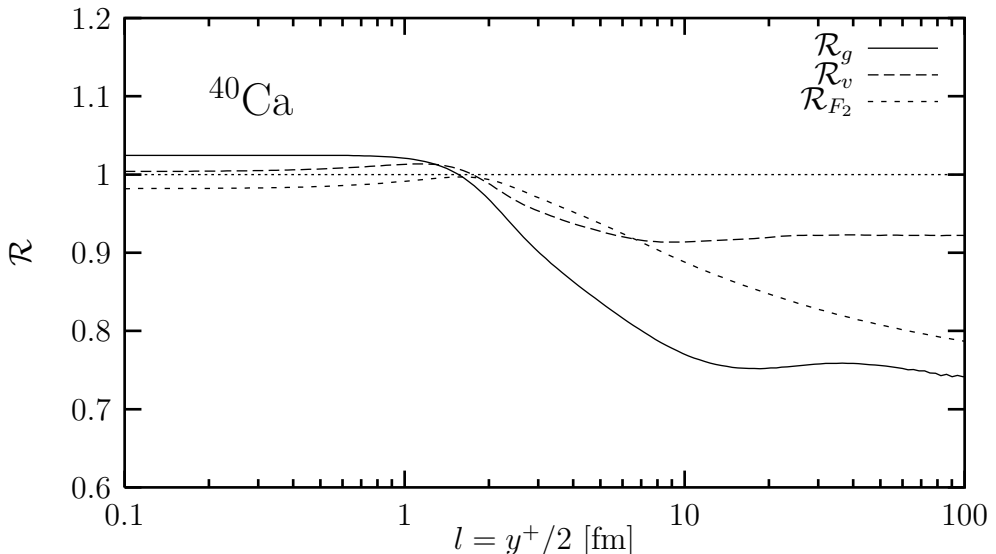


Figure 2. Ratios of nuclear (^{40}Ca) and free nucleon coordinate space distributions for gluons (solid), valence quarks (dashed) and for the structure functions $F_2^{A,N}$ (dotted) at $Q^2 = 4 \text{ GeV}^2$. For further details see ref. [3].

3. Partons versus hadrons: generalized nucleon polarizabilities

At intermediate $Q^2 \lesssim 1 \text{ GeV}^2$ a detailed analysis of virtual Compton scattering on the nucleon should provide insights into the transition from partonic to hadronic degrees of freedom in the nucleon. Interesting quantities to look at in this context are the generalized (Q^2 -dependent) electromagnetic polarizabilities. We investigate:

- a) the sum of electric and magnetic polarizabilities

$$\Sigma(Q^2) = (\alpha + \beta)_{Q^2} = \frac{1}{2\pi^2} \int_{\omega_0}^{\infty} \frac{d\omega}{\omega^2} \sigma_T(\omega, Q^2), \quad (5)$$

where $\sigma_T(\omega, Q^2)$ denotes the total cross section for scattering of a transverse virtual photon at fixed $Q^2 = \vec{q}^2 - \omega^2 > 0$ from a nucleon, and the integration is taken over the photon energy ω from (pion-production) threshold to infinity. The ω^{-2} weighting in

this polarizability integral focuses on the low energy part of the excitation spectrum, but probed over a certain range of "resolution" Q^2 ;

b) the spin polarizability

$$\gamma(Q^2) = \frac{1}{4\pi^2} \int_{\omega_0}^{\infty} \frac{d\omega}{\omega^3} [\sigma_{1/2}(\omega, Q^2) - \sigma_{3/2}(\omega, Q^2)] \quad (6)$$

which involves the difference of helicity 1/2 and 3/2 photon-nucleon cross sections, accessible by polarized electroproduction measurements on the nucleon at fixed Q^2 . This polarizability has a characteristic ω^{-3} weighting under the integral. We recall that the corresponding integral with ω^{-1} gives the Gerasimov-Drell-Hearn sum rule.

In the limit of large Q^2 , the polarizabilities $\Sigma(Q^2)$ and $\gamma(Q^2)$ turn into certain moments of the structure functions F_1 and g_1 measured in unpolarized and polarized deep-inelastic lepton-nucleon scattering:

$$\Sigma(Q^2) \longrightarrow \frac{2e^2 M}{\pi Q^4} \int_0^1 dx \frac{x}{1-x} F_1(x), \quad (7)$$

$$\gamma(Q^2) \longrightarrow \frac{4e^2 M^2}{\pi Q^6} \int_0^1 dx \frac{x^2}{1-x} g_1(x). \quad (8)$$

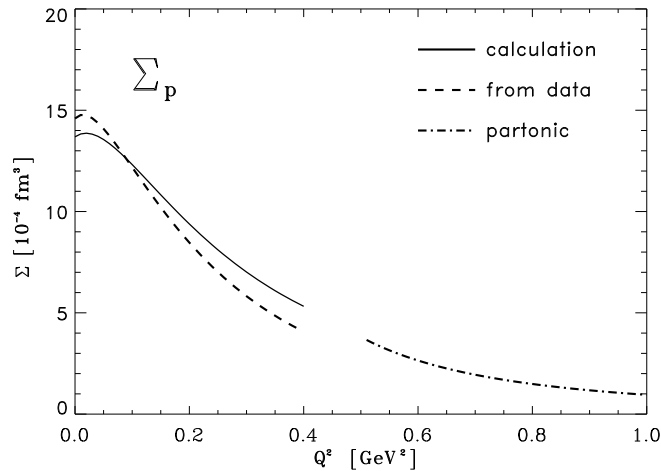


Figure 3. Generalized proton electromagnetic polarizability $\Sigma_p(Q^2)$ (see text and ref. [5]). The calculated full line includes relativistic pion loops and the $\Delta(1232)$ resonance. Data (dashed) from inelastic electron-proton scattering. Dash-dotted curve: partonic description using the structure function F_1 .

The interesting question is then the following: how does the QCD description of $\Sigma(Q^2)$ and $\gamma(Q^2)$ in terms of quarks and gluons at large Q^2 turn into the hadronic low Q^2 description of the same quantities? At low Q^2 , QCD with light (u-, d- and s-) quarks translates into a chiral effective Lagrangian of Goldstone bosons (pions, kaons,...) coupled to baryons and vector mesons. This effective field theory has been used [5] at the level

of one-loop chiral perturbation theory in the pion-nucleon sector to evaluate the nucleon polarizabilities $\Sigma(Q^2)$ and $\gamma(Q^2)$ for $Q^2 \lesssim 0.5 \text{ GeV}^2$. This framework emphasizes the role of the pion cloud and the $N \rightarrow \Delta$ excitation of the nucleon in response to the electromagnetic field.

At high Q^2 , on the other hand, nucleon structure is realised in terms of its parton (quark and gluon) content. We have explored whether low- Q^2 chiral dynamics matches high- Q^2 partonic structure in $\Sigma(Q^2)$ and $\gamma(Q^2)$. The results [5] are presented in Figs. 3, 4. Let us first discuss the Q^2 -dependent electromagnetic polarizability Σ_p of the proton (Fig. 3). The chiral dynamics calculation (solid line) summarizes the response of the pion cloud and through resonance (primarily $\Delta(1232)$) excitation and compares very well with the data (dashed curve) derived from inelastic electron scattering in the range $Q^2 \lesssim 0.5 \text{ GeV}^2$. The downward extrapolation of the parton distribution F_1 from deep-inelastic scattering (dash-dotted curve) determines $\Sigma(Q^2)$ at large Q^2 . Both descriptions evidently meet at intermediate Q^2 , indicating a smooth crossover from partonic to hadronic degrees of freedom.

The result for the Q^2 -dependent spin polarizability has similar features (Fig. 4). On the low- Q^2 side we see the well-known balance between the diamagnetic response of the pion cloud and the spin-paramagnetic effect of the $N \rightarrow \Delta$ (spin 1/2-to-spin 3/2) transition. Dia- and paramagnetism enter with opposite signs and comparable magnitudes, so that the resulting $\gamma(Q^2)$ is small and changes sign at $Q^2 \simeq 0.4 \text{ GeV}^2$. The downward extrapolation from high Q^2 can be made using the spin structure function g_1 from polarized deep-inelastic scattering. Again it matches the low- Q^2 hadronic calculation remarkably well.

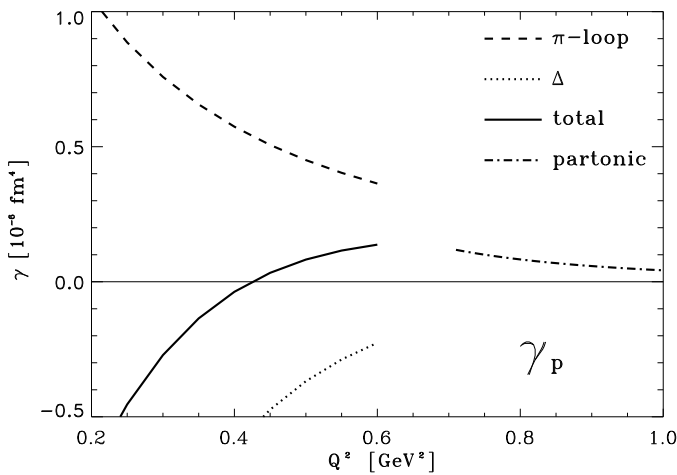


Figure 4. generalized proton spin polarizability $\gamma(Q^2)$ as calculated in ref. [5]. Pion loop (diamagnetic) and Δ resonance (paramagnetic) contributions are shown separately. Their sum (solid curve) is compared with the partonic prediction using the spin structure function g_1 .

4. Low-energy QCD with strange quarks: Chiral $SU(3)$ Dynamics

QCD with massless u-, d- and s-quarks has a chiral $SU(3)_L \times SU(3)_R$ symmetry. As a consequence of strong QCD forces this symmetry is spontaneously broken. It is also explicitly broken by the quark masses. The symmetry breaking pattern is manifest in the low-energy hadron spectrum, with the light pseudoscalar mesons representing the Goldstone bosons of the spontaneously broken symmetry. The strange quark is special since its mass is intermediate between "light" and "heavy". One of the key questions is then the following: to what extent do the *symmetries* of QCD govern strong interaction *dynamics*, and what is the role of the strange quark in this context?

Progress has recently been made in developing a framework to deal with these problems. The starting point is the chiral effective Lagrangian, a theory of Goldstone bosons (pions, kaons and eta mesons) coupled to the octet of baryons. It is designed according to the rules set by QCD symmetries [6]. This effective Lagrangian introduces a characteristic scale, $4\pi f_\pi \sim 1 \text{ GeV}$, where $f_\pi = 92.4 \text{ MeV}$ is the pion decay constant.

Spontaneously broken chiral symmetry also implies that the low-energy interactions of Goldstone bosons are weak: the leading behaviour of any amplitude for scattering of a pseudoscalar meson on a baryon goes like

$$T_{\text{meson-baryon}} = \text{const} \cdot \frac{E}{f_\pi^2} + \dots, \quad (9)$$

where E is the meson energy in the center-of-mass system. The constant in eq. (9) is specific for each meson-baryon channel and completely determined by $SU(3)$ symmetry. Pions close to threshold with $E \simeq m_\pi$ have small scattering amplitudes. In this case chiral perturbation theory (ChPT), the systematic expansion of observables in powers of energy of momentum (or m_π) is a useful concept. When strange quarks are involved, the scattering amplitudes scale as E/f_π^2 with $E \geq m_K$, and the driving terms in (9) become sizable. One therefore expects that ChPT is only of limited value once strangeness is included. A way to proceed which proves to be quite successful is chiral $SU(3)$ dynamics [7]: a non-perturbative coupled-channel approach based on the chiral $SU(3) \times SU(3)$ effective meson-baryon Lagrangian. The basic strategy is first to generate Born terms $T_{ij}^{(0)}$ of the multi-channel meson-baryon T-matrix from the chiral effective Lagrangian and then to perform a partial loop summation to all orders using a Lippmann-Schwinger equation:

$$T = [1 - T^{(0)} \cdot G]^{-1} T^{(0)}, \quad (10)$$

with an appropriate Green function G . Introducing a limited number of finite-range parameters, a remarkably good description of a large amount of cross section can be achieved. This method has been successfully applied [7] to KN scattering, the coupled $\{\bar{K}N, \pi Y, \eta Y\}$ and $\{\pi N, KY, \eta N\}$ multi-channel systems, and to the photoproduction of η and K mesons. Simplified but otherwise very similar calculations are reported elsewhere at this conference [8].

While all previous calculations have dealt with s -wave dynamics, the present focus is on the systematic incorporation of p -waves as required by a multitude of measured meson-baryon angular distributions and polarization observables. We have now reached

the stage where the complete s - and p -wave chiral $SU(3)$ dynamics is well under control [9]. As an example Fig. 5 shows predicted cross sections for kaon photoproduction once a limited set of parameters has been fixed to reproduce a large variety of $\pi N \rightarrow \eta N$, $K\Lambda$ and $K\Sigma$ cross sections and angular distributions. The $l = 1$ partial waves are evidently important in such channels immediately above threshold. With the inclusion of p -waves, further detailed tests of the chiral $SU(3)$ effective Lagrangian are now possible.

A forthcoming necessary step is to incorporate the axial $U(1)$ anomaly and the dynamics of the η' . This is where the gluonic sector of QCD should have its impact.

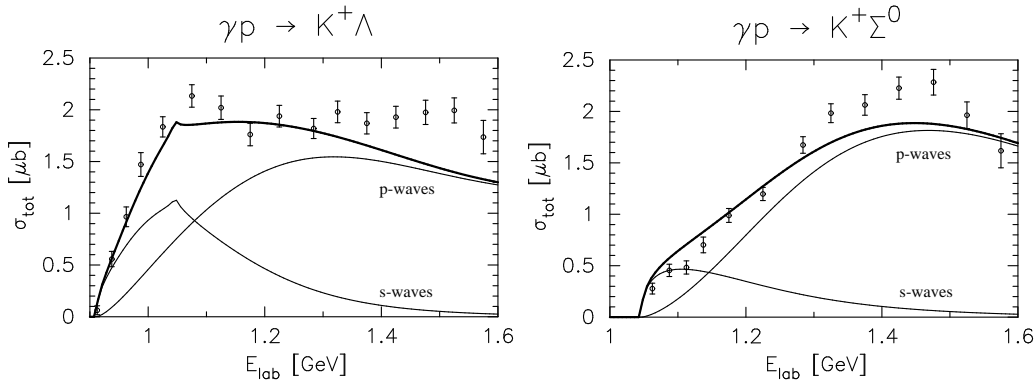


Figure 5. Kaon photoproduction cross sections using s - and p -wave chiral $SU(3)$ dynamics [9], a non-perturbative coupled channel approach based on the chiral meson-baryon Lagrangian [7]. The data are taken from ref. [10].

5. QCD Sum Rules: some recent developments

The QCD sum rule method of treating the non-perturbative dynamics of QCD was developed twenty years ago (SVZ sum rules [11]). It connects the expansion of a correlation function in terms of vacuum condensates (the operator product expansion) with the spectrum of this correlation function via dispersion relations. These sum rules have been applied to understand the masses and properties of a variety of hadrons emphasizing their role as excitations of the condensed QCD vacuum.

QCD sum rules have also been used in more recent times to arrive at estimates for possible in-medium mass shifts of vector mesons [12]. The validity of such estimates has been under debate, however, for several reasons. Uncertainties exist at the level of factorization assumptions used to approximate four-quark condensates $\langle \bar{q}\Gamma q \bar{q}\Gamma q \rangle$ in terms of $\langle \bar{q}q \rangle^2$, the square of the standard chiral condensate. Furthermore, for broad structures such as the ρ meson, with its large vacuum decay width further magnified by in-medium reactions, the QCD sum rule analysis does not provide a reliable framework to extract a "mass shift" in medium. The situation is more comfortable for the ω meson which has a vacuum width twenty times smaller than that of the ρ meson and may have a much better chance to survive as a quasi-particle in nuclear matter [13].

We have recently re-examined these questions [14] in search for model-independent sum-rule constraints which do not suffer from the uncertainties introduced by four-quark condensates. We exemplify these constraints for the case of the ω meson spectral distribution and its changes in the nuclear medium.

The starting point is the current-current correlation function

$$\Pi_{\mu\nu}(q) = i \int d^4x e^{iq\cdot x} \langle \mathcal{T} j_\mu(x) j_\nu(0) \rangle = \left(\frac{q_\mu q_\nu}{q^2} - g_{\mu\nu} \right) \Pi(q^2), \quad (11)$$

and we work with the spectrum

$$R(s) = \frac{12\pi}{s} \text{Im} \Pi(s). \quad (12)$$

In vacuum $R(s)$ is directly related to $\sigma(e^+e^- \rightarrow \text{hadrons})$. In dense and hot hadronic matter it enters into the analysis of lepton pair production in high-energy heavy-ion collisions.

One proceeds now as follows. First $\Pi(q^2)$ is expanded at large spacelike q^2 (i. e. for $Q^2 = -q^2$ positive and large) in powers of $1/Q^2$ using the QCD operator product expansion. At the same time $\Pi(q^2)$ is written in the form of a dispersion relation. Then a Borel transformation is performed which effectively reduces the weight on the uncertain high-energy parts of the spectrum. Let us focus on the ω meson with the isoscalar current $j_\mu = \frac{1}{6}(\bar{u}\gamma_\mu u + \bar{d}\gamma_\mu d)$ and discuss the vacuum case first. One finds

$$\int_0^\infty ds R(s) e^{-s/\mathcal{M}^2} = \frac{1}{6} \left(1 + \frac{\alpha_s}{\pi} \right) \mathcal{M}^2 + \frac{C}{\mathcal{M}^2} + \dots \quad (13)$$

where the Borel mass \mathcal{M} is a technical scale parameter and C is a combination of quark and gluon condensates:

$$C = \frac{2\pi^2}{3} \left(\langle m_u \bar{u}u + m_d \bar{d}d \rangle + \frac{1}{12} \langle \frac{\alpha_s}{\pi} G_{\mu\nu} G^{\mu\nu} \rangle \right). \quad (14)$$

A negligibly small quark mass term has been dropped on the r.h.s. of eq. (13). Terms of order \mathcal{M}^{-4} involve combinations of (uncertain) four-quark condensates. In a nuclear medium the condensate term (14) receives density-dependent corrections, the leading one being proportional to the first moment of the quark distribution in the nucleon.

The vacuum spectrum of the ω meson has the characteristic behaviour shown in Fig. 6: a resonant part below a scale s_0 followed by a continuum $R_c(s)$ which approaches the perturbative QCD limit for $s > s_0$:

$$R_c \simeq \frac{1}{6} \left(1 + \frac{\alpha_s}{\pi} \right) \Theta(s - s_0). \quad (15)$$

Splitting the spectrum into resonance and continuum and choosing $\mathcal{M} > \sqrt{s_0}$, a term-by-term comparison in eq. (13) gives a set of sum rules for the moments of $R(s)$. The lowest ones (in vacuum) are

$$\int_0^{s_0} ds R(s) = \frac{s_0}{6} \left(1 + \frac{\alpha_s}{\pi}\right), \quad (16)$$

$$\int_0^{s_0} ds s R(s) = \frac{s_0^2}{12} \left(1 + \frac{\alpha_s}{\pi}\right) - C, \quad (17)$$

with the condensate term C of eq. (14). Higher moments of $R(s)$ successively introduce condensates of higher dimensions.

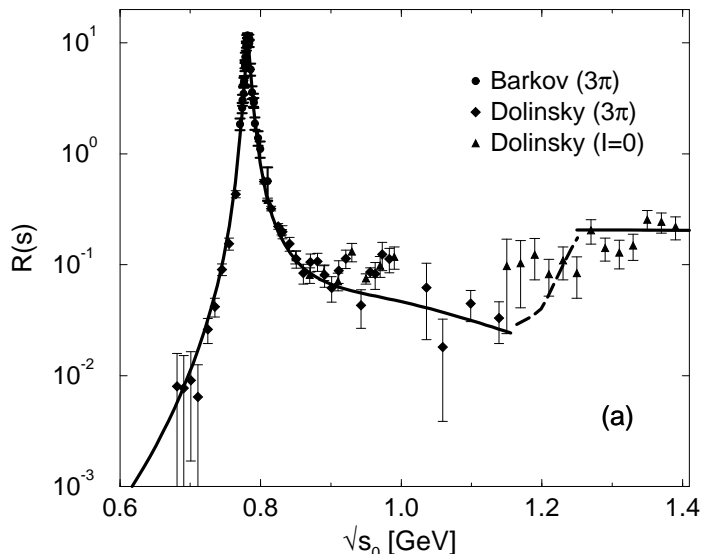


Figure 6. Spectrum $R(s)$ in the ω meson channel as calculated in ref. [13,14]. The data points refer to $e^+e^- \rightarrow 3\pi$ and $e^+e^- \rightarrow$ hadrons ($I = 0$).

Let us now make an attempt to unify QCD sum rules with chiral symmetry and current algebra. Recall that the scale for spontaneous chiral symmetry breaking, $\Delta = 4\pi f_\pi \sim 1 \text{ GeV}$, is realized as a characteristic gap in the low-mass hadron spectrum. The light vector mesons are the lowest $q\bar{q}$ dipole ($J^\pi = 1^-$) excitations of the QCD vacuum, with their masses located just under the gap Δ .

We propose [14] that the scale $\sqrt{s_0}$ which separates the hadronic (resonance) sector from the quark-antiquark continuum in the QCD sum rule analysis, should be identified with the gap Δ , setting

$$\sqrt{s_0} = \Delta = 4\pi f_\pi. \quad (18)$$

That this makes some sense can be seen instantly by returning to the Vector Meson Dominance (VMD) model for the resonant part of $R(s)$. In this model, taking the zero

width limit, we have

$$R(s) = \frac{4\pi^2}{3} \frac{m_\omega^2}{g^2} \delta(s - m_\omega^2) + R_c(s) \quad (19)$$

with the vector coupling constant $g \simeq 6$. From the sum rule (16) one finds

$$\frac{8\pi^2}{g^2} \frac{m_\omega^2}{s_0} = 1 + \frac{\alpha_s}{\pi}. \quad (20)$$

In fact this equation holds both for ω and ρ meson in the zero width limit, with degenerate masses $m_V = m_\rho = m_\omega$. Inserting $s_0 = 16\pi^2 f_\pi^2$ one immediately recovers the celebrated current algebra (KSFR) relation

$$m_V = \sqrt{2} g f_\pi, \quad (21)$$

apart from a small perturbative QCD correction. Note that the second sum rule (17) gives the interesting further constraint $g = 2\pi$ (up to small α_s and condensate corrections which drive g closer to its empirical value).

The in-medium downward shift of the vector meson mass in the zero-width limit found in ref. [12] was about 15 % at nuclear matter density, $\rho = \rho_0 = 0.17 \text{ fm}^{-3}$, and came primarily through the downward shift of s_0 in the QCD sum rule analysis. With the identification (18) in the dipole sum rules (16, 17), this can now be easily understood in terms of the in-medium reduction of the gap $\Delta(\rho) = 4\pi f_\pi(\rho) = \sqrt{s_0(\rho)}$. The pion decay constant (in fact, the one related to the time component of the axial current in hadronic matter) is proportional to the square root of the chiral condensate $\langle \bar{q}q \rangle$. Its leading dependence on baryon density is controlled by the nucleon sigma term $\langle N|\bar{q}q|N \rangle$ which induces an approximate 30 % reduction of the magnitude of $\langle \bar{q}q \rangle$ at $\rho = \rho_0$.

While such relationships are obscured for the ρ meson by its very large in-medium width, they may well be realized for the much narrower ω meson. In fact explicit calculations [13] of the in-medium ω meson spectrum using the chiral $SU(3) \times SU(3)$ Lagrangian with inclusion of anomalous couplings from the Wess-Zumino action, turn out to be fully consistent with the QCD sum rule analysis. The suggested in-medium mass shift may even lead to nuclear bound states of ω mesons [15,16], an exciting perspective.

REFERENCES

1. P. Hoyer and M. Vänttinen, Z. Phys. **C 74** (1997) 113; B. L. Ioffe, Phys. Lett. **B 30** (1969) 123.
2. H. L. Lai et al., Phys. Rev. **D 55** (1997) 1280
3. M. Vänttinen, G. Piller, L. Mankiewicz, W. Weise and K. J. Eskola, Eur. Phys. J. **A 3** (1998) 351.
4. L. Frankfurt, M. Strikman and S. Liuti, Phys. Rev. Lett. **65** (1990) 1725; K. J. Eskola, Nucl. Phys. **B 400** (1993) 240; K. J. Eskola, V. J. Kolhinen and P. V. Ruuskanen, hep-ph/9802350, Nucl. Phys. B (to appear).
5. J. Edelmann, N. Kaiser, G. Piller and W. Weise, Nucl. Phys. **A 641** (1998) 119.

6. see e. g.: V. Bernard, N. Kaiser and U.-G. Meißner, *Int. J. Mod. Phys. E* **4** (1995) 193.
7. N. Kaiser, P. B. Siegel and W. Weise, *Nucl. Phys. A* **594** (1995) 325; N. Kaiser, T. Waas and W. Weise, *Nucl. Phys. A* **612** (1997) 297.
8. E. Oset, this conference
9. J. Caro Ramón, N. Kaiser, S. Wetzel and W. Weise, preprint (1999), to be published.
10. M. Q. Tran et al., *Phys. Lett. B* **445** (1998) 20.
11. M. Shifman, A. Vainshtein and V. Zakharov, *Nucl. Phys. B* **147** (1979) 385; 448.
12. T. Hatsuda and S. H. Lee, *Phys. Rev. C* **46** (1992) R 34.
13. F. Klingl, N. Kaiser and W. Weise, *Nucl. Phys. A* **624** (1997) 527.
14. F. Klingl and W. Weise, *Eur. Phys. J. A* (1999), in print.
15. K. Tsushima, D. L. Lu, A. W. Thomas and K. Saito, *Phys. Lett. B* **43** (1998) 26.
16. F. Klingl, T. Waas and W. Weise, *Nucl. Phys. A* (1999), in print.